

# Imaging of the three-dimensional alveolar structure and the alveolar mechanics of a ventilated and perfused isolated rabbit lung with Fourier domain optical coherence tomography

## Alexander Popp

Medical Faculty of Technical University Dresden  
Clinical Sensing and Monitoring  
Fetscherstraße 74  
01307 Dresden, Germany  
E-mail: Alexander.popp@mailbox.tu-dresden.de

## Martina Wendel

Medical Faculty of Technical University Dresden  
Department of Anesthesiology and Intensive Care  
01307 Dresden, Germany

## Lilla Knels

Medical Faculty of Technical University Dresden  
Department of Anatomy and Department of  
Anesthesiology and Intensive Care  
01307 Dresden, Germany

## Thea Koch

Medical Faculty of Technical University Dresden  
Department of Anesthesiology and Intensive Care  
01307 Dresden, Germany

## Edmund Koch

Medical Faculty of Technical University Dresden  
Clinical Sensing and Monitoring  
01307 Dresden, Germany

**Abstract.** In this feasibility study, Fourier domain optical coherence tomography (FDOCT) is used for visualizing the 3-D structure of fixated lung parenchyma and to capture real-time cross sectional images of the subpleural alveolar mechanics in a ventilated and perfused isolated rabbit lung. The compact and modular setup of the FDOCT system allows us to image the first 500  $\mu\text{m}$  of subpleural lung parenchyma with a 3-D resolution of  $16 \times 16 \times 8 \mu\text{m}$  (in air). During mechanical ventilation, real-time cross sectional FDOCT images visualize the inflation and deflation of alveoli and alveolar sacks (acini) in successive images of end-inspiratory and end-expiratory phase. The FDOCT imaging shows the relation of local alveolar mechanics to the setting of tidal volume (VT), peak airway pressure, and positive end-expiratory pressure (PEEP). Application of PEEP leads to persistent recruitment of alveoli and acini in the end-expiratory phase, compared to ventilation without PEEP where alveolar collapse and reinflation are observed. The imaging of alveolar mechanics by FDOCT will help to determine the amount of mechanical stress put on the alveolar walls during tidal ventilation, which is a key factor in understanding the development of ventilator induced lung injury (VILI). © 2006 Society of Photo-Optical Instrumentation Engineers. [DOI: 10.1117/1.2162158]

Keywords: medical imaging; biomedical optics; coherence; tomography; interferometers; imaging.

Paper 05131R received Jun. 3, 2005; revised manuscript received Aug. 13, 2005; accepted for publication Sep. 2, 2005; published online Jan. 24, 2006. This paper is a revision of a paper presented at the SPIE conference on Optical Coherence Tomography and Coherence Techniques II, Jun. 2005, Munich, Germany. The paper presented there appears (unrefereed) in SPIE Proceedings Vol. 5861.

## 1 Introduction

Optical coherence tomography (OCT)<sup>1</sup> is an emerging image modality in medical diagnosis and biomedical research. Because OCT is still a relatively young technique, there is a vital search for new potential applications exploiting the capability of OCT to provide high-resolution subsurface structural information. A very interesting organ that calls for the depth visualization capabilities of OCT is the ventilated lung with its delicate structure of interconnected aerated alveoli and alveolar ducts. Because the measurement speed of OCT systems is constantly improved, time-resolved image capture of alveolar mechanics during the different phases of the ventilation cycle become possible. In this feasibility study, the 3-D alveolar structure of fixated rabbit lungs and the alveolar mechanics of ventilated and perfused rabbit lungs are visualized with a Fourier domain OCT system. The aim of the study is to introduce OCT as an investigative tool for alveolar mechanics, which in

contrast to surface microscopy provides depth information about subpleural alveoli. The main motivation for studying alveolar mechanics is given in the context of ventilator-induced lung injury, which frequently occurs during the treatment of severe critical illness affording mechanical ventilation.

### 1.1 Clinical Background: Role of Alveolar Mechanics in Ventilator Induced Injury

The acute respiratory distress syndrome (ARDS) is a severe form of acute lung injury resulting from sepsis, trauma, or severe pulmonary infections. Intensive care management of ARDS and acute lung injury (ALI) frequently requires endotracheal intubation and mechanical ventilation of the patients to ensure sufficient blood oxygenation.<sup>2</sup> The mechanical ventilation itself, although life saving, eventually has negative side-effects on the lung. As soon as there was a consensus that the ventilation contributes to or exacerbates ARDS by causing ventilator induced/associated lung injury (VILI/VALI),<sup>3</sup> an ongoing search for more protective forms of ventilation

Address all correspondence to Alexander Popp, Klinisches Sensing und Monitoring, Medizinische Fakultät der TU Dresden, Fetscherstr. 74, Dresden, Dresden 01307 Germany. Tel: +49 351 458 6131; Fax: +49 351 458 6325; E-mail: alexander.popp@mailbox.tu-dresden.de

started. As demonstrated in clinical studies, ventilator settings with lower tidal volume (VT) and higher positive end-expiratory pressure (PEEP) than traditionally used lead to a better outcome and lower mortality of ARDS patients.<sup>4</sup>

To understand the positive effects of low volume and high PEEP ventilation and to develop new protective forms of ventilation, the mechanisms responsible for VILI/VALI have to be clarified in detail. The amount of stress (tensile strain and shear forces) put on the alveolar walls during ventilation is thought to be a key factor for the development of VILI.<sup>5</sup> Two main initial stress mechanisms have been suggested: 1. volutrauma caused by overdistension of the alveolar walls, and 2. atelectrauma associated with alveolar recruitment and derecruitment (R/D). The R/D mechanisms are controversially discussed. There is no agreement on the exact deformation of acini and alveoli during volume uptake and the corresponding stress put on the alveolar walls, even when looking at healthy lungs. A variety of mechanisms is discussed that are partly contradicting or hypothetical. Some researchers favor a balloon-like expansion of the alveoli, some suggest an expansion of alveolar ducts without changes of alveolar form and size in the normal lung, some describe R/D as repetitive alveolar collapse and opening or uncrumpling of folded alveoli and acini, others state that air bubbles being pressed through edemic (water filled) airways might induce the atelectrauma.<sup>6,7</sup>

## 1.2 Challenge: Imaging Alveolar Mechanics

The reason for the controversy about alveolar mechanics is mainly caused by the difficulties that arise when trying to image the alveoli *in situ* during ventilation. The interpretation of pressure-volume curves,<sup>8</sup> arterial fixation and histological examination of lungs at different tidal volumes,<sup>9</sup> inductance plethysmography, electrical impedance tomography,<sup>10</sup> and computed tomography scans<sup>11</sup> have all contributed to a better understanding of whole lung mechanics. However, they all do not provide the real-time information *and* spatial resolution that are necessary to analyze mechanics of aerated lungs on an alveolar scale during ventilation. Since the mid-1970s, videomicroscopy of subpleural alveoli has provided high-resolution information about lung mechanics on an alveolar scale.<sup>12</sup> More recently, the group of Nieman captured real-time *in-vivo* microscopic images of subpleural alveoli and presented a series of quantitative studies on alveolar mechanics in healthy and pathological lungs modeling ARDS.<sup>6,13</sup> But there is a principle drawback in using microscopy: it provides top views of alveoli through a glass plate sucked to the pleura. Thus, the information is only 2-D. This restricted view leaves questions open about the interconnectivity of the alveoli, about a possible anisotropy of volume expansion, and about such complex processes like the unfolding of acini. Because this depth information is missing in microscopy, there is still a search for “the ideal investigative tool,” which was defined as one “that can measure 3-D changes that occur in the alveolus and alveolar duct continuously throughout tidal ventilation.”<sup>6</sup>

## 1.3 Feasibility of Fourier Domain Optical Coherence Tomography for Imaging Alveoli

Our study aims at proving that optical coherence tomography (OCT), and especially its spectral domain variant Fourier do-

main OCT (FD-OCT),<sup>14,15</sup> is a potent tool for studying the dynamic mechanics of subpleural alveoli and acini during ventilation. In contrast to microscopy, OCT has the advantage of providing depth information from the first subsurface 500  $\mu\text{m}$  of highly scattering tissue with a resolution better than 10  $\mu\text{m}$ . This information is gained by analyzing the reflection of infrared probe light scattered by structures within the tissue. To extract the depth information of the scatterers, the echoed probe light is brought to interference with a reference light beam originating from the same low coherence light source. The principle of operation and the different variants of OCT, such as time domain OCT (TD-OCT), spectral/Fourier domain OCT (FD-OCT), linear OCT, and swept source OCT, are all described in review articles.<sup>16</sup> For high-speed applications, Fourier domain OCT seems most suitable because the analysis of the interference by a spectrometer requires neither mechanically moving parts in the reference arm nor frequency tuning of the light source. In fact, high-speed FD-OCT systems have recently achieved frame rates of 29.3/s for 2-D cross sectional imaging.<sup>17</sup> More and more, 3-D imaging OCT systems are reported to produce volume scans of complex 3-D structures like the spiral sweat glands in human skin.<sup>18</sup> The optical setup of the compact prototype FD-OCT system used in this feasibility study is described in Sec. 2.3.

## 1.4 Optical Coherence Tomography Imaging of the Lung

Its ability to provide depth information makes OCT a promising tool for tissue classification and tumor investigation. Thus, OCT has already been used in other feasibility studies for imaging excised lung tissue,<sup>19,20</sup> introducing OCT as a potential real-time alternative to histological investigation during thorax surgery. In another study, the dynamics of laser ablation of *ex-vivo* lung tissue, followed by the deflation of alveoli, was captured by OCT imaging with a 0.1-s time resolution.<sup>21</sup> Very recently, endoscopic OCT scanner heads of 1 mm diam were used to detect abnormalities in the diseased airway epithelium during *in-vivo* fiber optic bronchoscopy.<sup>22</sup> In the same study, *ex-vivo* cross sectional OCT imaging of the subpleural alveoli was performed on fixated lung tissue excised from pigs. To our knowledge, there has been no report so far on OCT imaging of alveolar mechanics during ventilation.

## 2 Materials and Methods

### 2.1 Isolated Rabbit Lung

The model of the ventilated and blood-free perfused isolated rabbit lung has been already used by our group for studies on ventilator-induced injury, and is therefore an appropriate model for the testing of OCT imaging.<sup>23</sup> The protocol of this study is in accordance with the National Institutes of Health guidelines for animal use. The preparation of the isolated, perfused rabbit lung model has been described in detail by our group elsewhere.<sup>24</sup> Briefly, female rabbits (*Orctolagus cuniculus*) weighing 2.2 to 3.2 kg were anesthetized with ketamine 50 mg/kg (CuraMED, Karlsruhe, Germany) and xylazine hydrochloride 4 mg/kg (Bayer, Leverkusen, Germany) after cannulation of the auricular vein. Anticoagulation was

**Table 1** Ventilator settings for the isolated rabbit lung.

Time (min)	10	20	30	40	50	60
PEEP (cm H <sub>2</sub> O)	5	5	5	0	0	0
VT (mL/kg)	10	12	15	10	12	15

achieved by means of IV administration of heparin 1000 U/kg (Liquemin, Hoffman-La Roche, Grenzach-Wyhlen, Germany). After pretracheal infiltration with 8 mL of lidocaine hydrochloride 1% (Jenapharm, Jena, Germany), a tracheotomy was performed, and the trachea was cannulated by using a 10-cm-long catheter with a diameter of 0.4 cm (endotracheal tube) (B. Braun, Melsungen, Germany). Animals had the lungs ventilated with room air by use of a mechanical ventilator equipped with a serial interface (Cato, Dräger, Lübeck, Germany). The real-time pressure data were transmitted to the OCT controlling personal computer via RS232 serial bus using a real-time protocol (MEDIBUS, Dräger, Lübeck, Germany). The initial ventilator settings were  $V_t=8$  mL/kg, respiratory frequency=30 breaths/min, PEEP=5 cm H<sub>2</sub>O, and inspiratory-expiratory ratio 1:1. After a median sternotomy, the pulmonary artery was cannulated, and perfusion with Krebs-Henseleit hydroxyethyl starch buffer solution (buffered with 20-mM HEPES at pH=7.35) started with a roller pump at 50 mL/min (Masterflex L/S, Cole-Parmer, Manufacturing, Barnant, Barrington, Illinois). Simultaneously, the heart was opened to permit the exsanguination of the lungs. The lungs and trachea were carefully dissected, removed en bloc, and suspended from a weight transducer (Hottinger Baldwin Messtechnik, Darmstadt, Germany) in a temperature-controlled (37 °C) double-walled chamber, which could be moved down to free the lung surface for OCT measurement. The lung perfusate dropping from the lungs into the chamber was collected into a reservoir and redirected to the roller pump as a closed recirculation system. The total volume of perfusate in the system was 200 mL. The temperature of the perfusate was maintained at 37 °C with a water bath, and weight gain was continuously recorded.

The respiratory frequency was lowered to 12/min and the inspiratory-expiratory ratio was changed to 1:1.5 before a series of six different ventilator settings, each lasting a time period of 10 min, was applied to the isolated lung (Table 1). OCT measurements were performed at the upper and lower lobe of the left lung at the second half of each time period.

## 2.2 Formalin-Fixated Rabbit Lung and Scanning Electron Microscopy

The lung was prepared as described in the previous section, disconnected from ventilation, and connected to a formalin reservoir. The lung was filled endobronchially with 4% formalin buffered solution with a pressure of 20-cm H<sub>2</sub>O, leading to an extension that is equivalent to the end-inspiratory size during ventilation. 20 minutes after starting the fixation and keeping the filling pressure constant, a series of 3-D OCT scans was taken.

Approximately 1 h after starting the fixation, the lungs were ligated at the trachea, disconnected from the reservoir,

and placed in 4% formalin solution for several days. Small probes of the lungs at the sites corresponding to OCT measurements were excised and washed three times with 0.1-M phosphate buffer solution (PBS). Dehydration of the lung was performed by a series of ethanol baths with increasing concentration (70% ethanol overnight, 80% for 1 h, 90% for 1 h, 96% for 30 min, and 3 × 20 min 100%). After critical point drying with liquid CO<sub>2</sub> (E3000, Gala Instruments, Schwalbach, Germany) and sputtering with gold in a Balzers MED010 sputtercoater (90 s, 50 mA), specimens were studied with a LEO 5430 scanning electron microscope.

## 2.3 Setup of the Common Path Fourier Domain Optical Coherence Tomography System

The optical setup [Fig. 1(a)] of the FD-OCT system used for alveolar imaging is based on a low coherent light source, which is a broadband near-infrared superluminescent diode (SLD) with a 50-nm-wide spectrum centered at 830 nm. One milliwatt of the SLD output power is coupled into a single-mode optical fiber. After passing a fiber coupler joining the pathways to the SLD and to the spectrometer, the light is guided to a handheld scanner head. In the scanner head, the light is collimated to a free space beam and deflected by a dichroitic mirror, reflective for infrared and transparent for visible light. This mirror is mounted on a galvanometer scanner providing fast beam deflection. The deflected beam is focused on the probe by telecentric optics. Close to the focal plane, the beam passes a partially reflective glass window. The reflective side of this window serves as the reference plane for the OCT interferometer. Between the reference window and the probe, an index matching gel is used to minimize first surface reflections by the probe. The light reflected by scattering structures within the probe, together with the reference light, is focused back into one common fiber and guided via the fiber coupler into the grating spectrometer, where the dispersed light is focused on a silicon line detector with a width of 1024 pixels. The resulting interference spectrum is read out to a personal computer at a maximum rate of 5 MHz by a 12-bit analog-digital converter.

The depth information of the scattering structures in the probe along the axial ( $z$ ) direction (A scan) is derived from the fast Fourier transformation of the spectrum. The axial measuring depth into the lung is limited by scattering to approximately 500  $\mu$ m, and the axial resolution in air is 8  $\mu$ m. One B-mode OCT image of 1200 × 512 pixels is acquired by collecting successive A scans and translating the logarithmized intensity values into grayscale levels while scanning a lateral extension of 6 mm.

A small complementary metal-oxide semiconductor (CMOS) camera behind the dichroitic scanner mirror allows

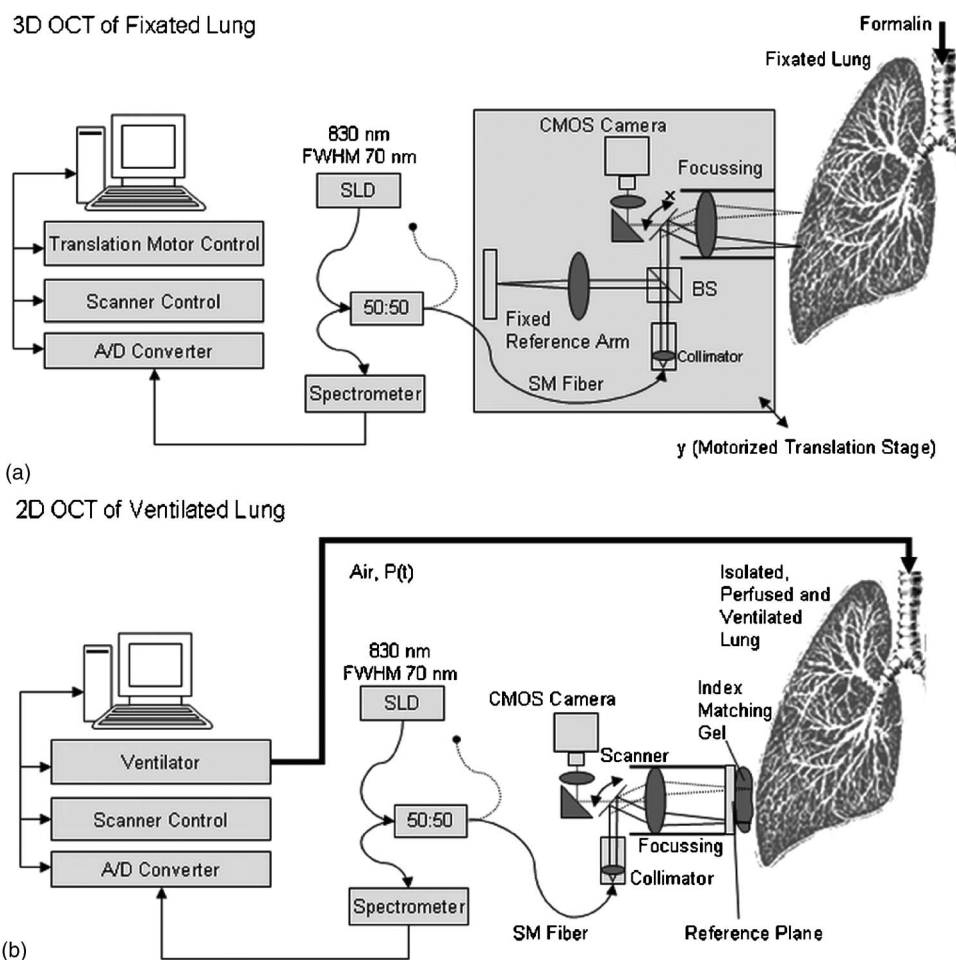


**Fig. 1** Setup of the FD-OCT system used for (a) (top) 3-D imaging with an OCT scanner head mounted on a y-translation stage. The scanner head contains a beamsplitter cube and a reference arm. The translation stage is controlled synchronously to image acquisition (b) (bottom) real-time 2-D imaging with a scanner head containing a partially reflective outlet window. The pressure of the mechanical ventilation is synchronously monitored. Index matching gel is put between pleura and outlet window.

monitoring of the surface of the probe and the moving beam spot, so disturbing air bubbles in the index matching gel can be detected and removed. Scanner control, data acquisition of OCT spectra, real-time acquisition of the ventilator pressure, and image processing are all implemented in a LabView® (National Instruments) program.

#### 2.4 Setup of the Contact-Free 3-D Optical Coherence Tomography

For the acquisition of 3-D OCT scans of the fixated lung, a modified OCT scanner has been used [Fig. 1(b)]. Instead of the partially reflective window at the outlet of the scanner head, a beamsplitter cube is introduced into the free space beam between the collimator and scanner mirror. The cube deflects 50% of the beam intensity into a reference arm with a focusing lens and a reference mirror. The reference mirror is adjusted at a fixed length in such a way that the optical pathway in the reference arm is approximately 1 mm longer than the optical pathway to the first surface in the probe arm. The depth of scattering structures is measured relative to the virtual reference plane within the tissue. In this geometry, first surface reflections are the most distant scattering signals pro-

ducing the highest modulation frequencies in the spectrum. Since the modulation transfer function of the line detector drops toward higher frequencies, the first surface reflections are damped compared to the scattering signals from deeper within the tissue. The focal plane can be adjusted independently, preferably in-between the surface and virtual reference plane. Because of the intrinsic reduction of first surface reflections, the use of index matching gel is not necessary in this setup.

To add the 3-D (y) perpendicular to the (x) deflection of the scanner mirror, the scanner head is mounted on a motorized translation stage with a maximum of 25-mm travel. The translation stage steps between successive B-mode scans, allowing the capture of a full 3-D volume scan of the tissue.

Since fixated lungs were used for 3-D imaging, measuring speed was not as crucial as in the real-time application. Consequently, a higher lateral resolution (16  $\mu\text{m}$ ) than in the 2-D measurements could be chosen and a 1250-kHz 16-bit analog/digital converter was used to collect the data. The B-mode image stacks were saved to the harddrive and processed off-line with a 3-D volume rendering program.

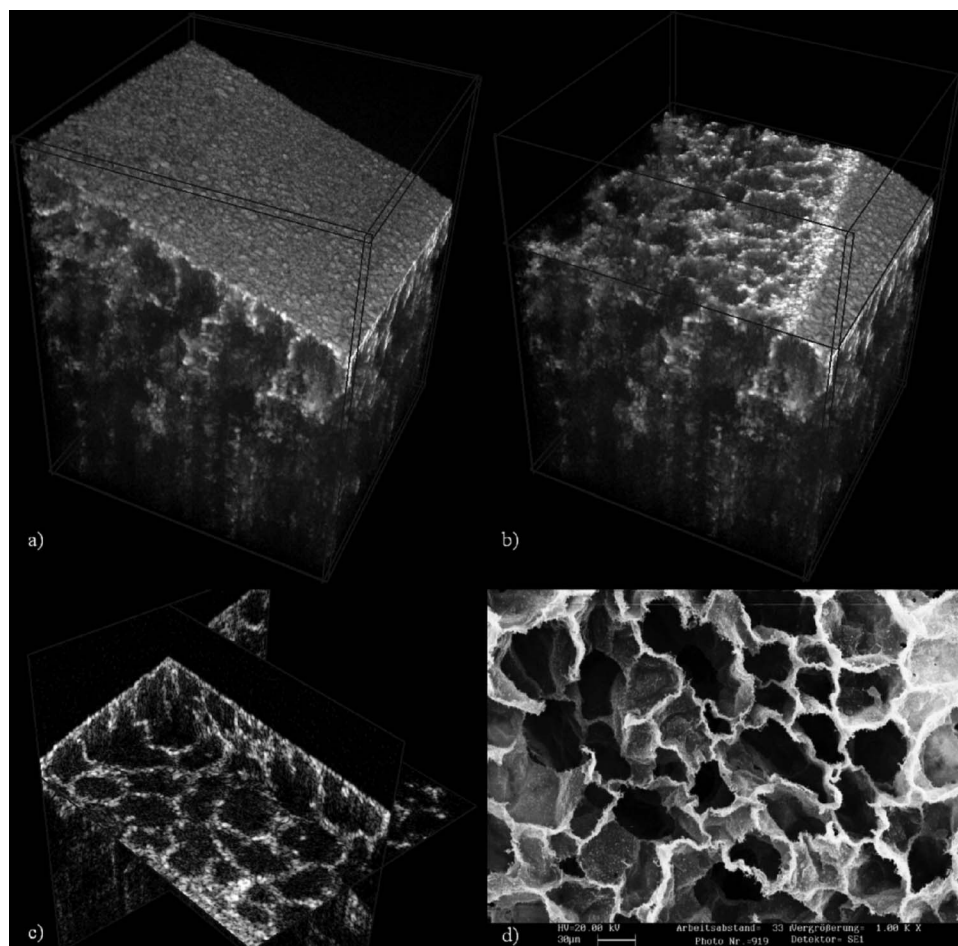


**Fig. 2** 3-D images of the formalin fixed rabbit lung. Volume rendered  $640 \times 640 \times 1024 \mu\text{m}$  (corrected with refractive index 1.3) scan in (a) (top left) full perspective view and (b) (top right) cut open parallel to an  $x$ - $y$  plane. (c) (bottom left) Three perpendicular cut planes in perspective view; lung parenchyma light, formalin filling dark. (d) (bottom right) SEM image for comparison.

### 3 Results

#### 3.1 Imaging of 3-D Alveolar Structure by Fourier Domain Optical Coherence Tomography

3-D OCT scans were taken from different spots at all lobes of a fixated rabbit lung immediately after fixation. In Figs. 2(a)–2(c) different views of a 3-D OCT scan of the upper right lobe are shown. The dimensions of the volume shown are  $640 \times 640 \times 1024 \mu\text{m}$  divided into  $256 \times 256 \times 256$  voxels with a size of  $2.5 \times 2.5 \times 4 \mu\text{m}$  (in air). The aspect ratio in the figures has been corrected for a refractive index of  $n=1.3$  to produce a realistic view. The pleural surface is tilted with respect to the  $x$ - $y$  plane of the scan. Figures 2(a) and 2(b) show volume-rendered projections of the OCT scan. In Fig. 2(b), a subpleural cut through the image data allows a view into the 3-D alveolar structure. The alveoli are filled with formalin, which produces much less scattering (black) than the lung parenchyma (light gray). In Fig. 2(c), three perpendicular cross sections are shown. The contour of individual subpleural alveoli can be clearly seen. The cross sections in the  $x$ - $y$  direction provide a homogeneous gray-level distribution, which is useful for further image processing (threshold conversion to black and white, tissue-surface to volume ratios, and 3-D segmentation).

#### 3.2 Correspondence of Fourier Domain Optical Coherence Tomography Images to Scanning Electron Microscope Images

To validate the quality of the 3-D OCT images, scanning electron microscope (SEM) images are compared to the OCT scans of the same lobe of the fixated lung. In Fig. 2(d), a SEM image shows a cut through the lung parenchyma. The OCT images of the fixated lung in Figs. 2(a)–2(c) qualitatively reproduce the shape and distribution of alveoli observed in the SEM image.

Because a different OCT scanner head was used for real-time imaging, a cross sectional OCT image (Fig. 3) taken of the fixated lung by this scanner is also compared to a SEM image (in the inset of Fig. 3) of a probe that was cut close to the pleura. The OCT image shows the pleura and cross sectional cuts through acini with individual alveoli. Again, the measured OCT depth data have been corrected for a refractive index of 1.3 to obtain a realistic aspect ratio in the image. The smaller average diameter of alveoli and alveolar ducts in the SEM image compared to the OCT image is due to a shrinking process taking place during the preparation procedure for the SEM imaging.

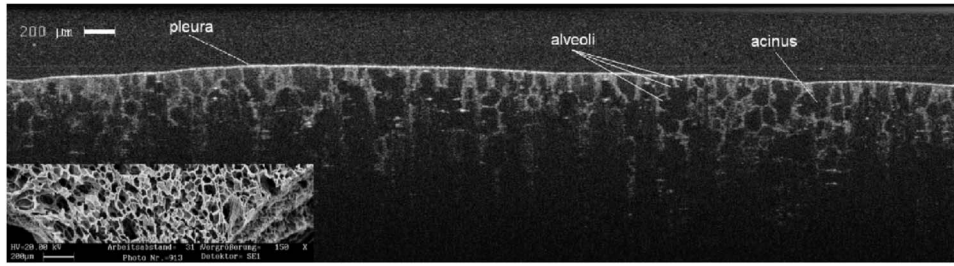


**Fig. 3** OCT cross sectional image ( $6 \times 2.1$  mm in air) of (a) (top) formalin fixed rabbit lung and in the inset a SEM image of the same scale. The height of the OCT image has been corrected for a refractive index of 1.3 to provide a realistic aspect ratio. The pleura, some individual alveoli, and an acinus (alveolar sack) are labeled. This image was acquired with the apparatus described in Fig. 1(b).

### 3.3 Real-Time Fourier Domain Optical Coherence Tomography Imaging of Alveoli throughout Tidal Ventilation

In Figs. 4(a)–4(d) two pairs of cross sectional B-mode OCT images of the upper left lobe of an isolated and blood-free perfused rabbit lung are shown. The acquisition time interval of one B scan (123 ms) is short compared to the inspiratory and expiratory phases of ventilation, allowing us to assign the

images to either of the ventilator phases and to omit images during transitional phases. In each pair there is one image captured at the end-inspiratory phase of ventilation and the other at the end-expiratory phase of mechanical ventilation. From pair to pair, different ventilator settings are applied. In Figs. 4(a) and 4(b), ventilator settings were  $VT=15$  mL/kg and  $PEEP=0$  cm  $H_2O$ . Figure 4(a) shows the end-inspiratory phase and Fig. 4(b) the end-expiratory phase of one ventilation cycle. In Figs. 4(c) and 4(d), ventilator settings were  $VT=10$  mL/kg and  $PEEP=5$  cm  $H_2O$ . Figure 4(c) shows the end-inspiratory phase and Fig. 4(d) the end-expiratory phase. For both ventilator settings, peak inspiratory airway pressure was 16-cm  $H_2O$ . The images cover a cross sectional area of  $6 \times 2.1$  mm with a resolution of  $20 \times 8 \mu m$  (in air). The simultaneously recorded pressure curves are plotted in the inserted bottom-left boxes with small circles indicating the point in time of the image acquisition.

In the images, light structures are assigned to lung parenchyma and dark areas are interpreted as cross sections of air filled volumes, i.e., alveoli and alveolar ducts.

In Fig. 4(a), air-filled (recruited) subpleural alveoli are present at end-inspiration and they are interconnected in the  $z$  direction to alveolar ducts. In Fig. 4(a), a pulmonary acinus with recruited alveoli is labeled. During the expiratory phase [Fig. 4(b)], the nonair-filled volume is increased, indicating that alveoli are derecruited and alveolar walls are folded [labeled in Fig. 4(b)] and there is low interconnectivity to alveolar ducts. These observations suggest that during inspiration, air flows from the distal airways into the alveoli, increasing the inner volume and expanding the walls of the acini. Looking at the change in shape and curvature of the walls surrounding the acini, one portion of the expansion might be due to expansion of individual alveolar walls, another part might be due to opening of additional alveoli (recruitment/derecruitment on an alveolar scale), and another portion might be due to an increase of the interconnecting volume (alveolar ducts). In a cross sectional view, however, the 3-D interconnectivity of the sliced volume is unknown, so the question remains if entire acini or only single alveoli are folded or crumbled during the non-PEEP expiratory phase and re-inflated during inspiration.

When PEEP is applied, the FD-OCT images of alveolar mechanics dramatically change. The corresponding images are shown in Figs. 4(c) and 4(d). In the inspiratory phase, more acini are aerated than in the non-PEEP case. In the expiratory phase, alveoli and acini stay open, indicating that

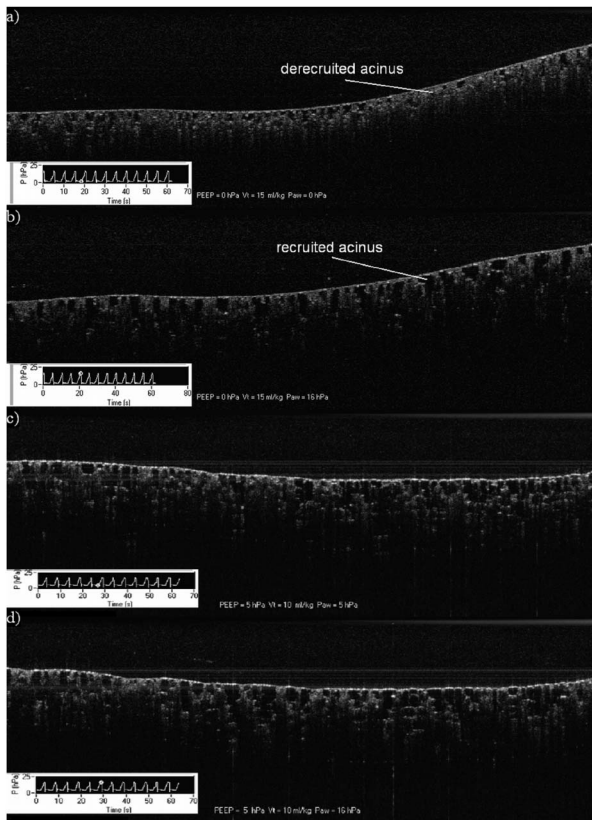


**Fig. 4** Cross sectional image series (top to bottom) of the ventilated isolated rabbit lung during (a) end-inspiratory phase of ventilation with  $VT=15$  mL/kg and zero PEEP; (b) corresponding end-expiratory image; (c) during end-inspiratory phase with  $VT=10$  mL/kg and  $PEEP=5$  hPa; and (d) corresponding end-expiratory phase. The airway pressures in (a) and (c) are both  $Paw=16$  hPa. In the insets, airway pressure versus time curves are shown; the circles indicate the time points of image acquisition. In the non-PEEP case, an acinus undergoing recruitment/derecruitment is labeled.

there is only little or no alveolar recruitment/derecruitment throughout the ventilatory cycle. In addition, there is more 2-D interconnectivity to alveolar ducts in the  $z$  direction compared to ventilation without PEEP.

In conclusion, the images in Figs. 4(a)–4(d) show that with the help of FD-OCT imaging, the influence of variations in VT and the effect of PEEP on the mechanics of the isolated lung can be visualized on an alveolar scale.

## 4 Discussion

OCT provides a unique view behind the pleura into the first 500  $\mu\text{m}$  of lung parenchyma. We demonstrate that the resolution of OCT images is sufficient to show individual alveoli. 3-D OCT of the lung parenchyma endobronchially filled with fixation solution reveals the full volume and shape information as well as the interconnectivity of alveoli. The comparison of OCT to SEM images proves that the structure of the lung parenchyma is realistically reproduced in the scattering intensity distribution of infrared light measured by OCT. This is an essential step toward a description of alveolar mechanics with OCT. Former studies on the 3-D structural changes of alveoli and acina during ventilation are all based on microscopic imaging of fixated lungs. This is the rationale for comparing OCT to the “gold standard.” Moreover, OCT might as well be used to validate the fixated lung approach itself. OCT could be used to monitor structural changes of the lung parenchyma during the various steps of the preparation process. Shrinking or any other geometrical changes from the ventilated state to a static aeration, fixation, and dehydration can be documented three dimensionally and nondestructively with OCT. This will fill the gap between the real *in-situ* geometry of ventilated alveolar structures and the geometry observed in the fixated probes. Artifacts introduced by the fixation process could be identified and corrected for. This way, OCT will help to ensure the authenticity of the 3-D geometrical information derived from fixated probes.

Using our fast-Fourier-type OCT system, we were able to acquire for the first time 2-D cross sectional images of ventilated subpleural alveoli in successive phases of the ventilator cycle in real time. Qualitatively, we observed R/D mechanisms at high tidal volume without PEEP, whereas persistent opening of the alveoli occurred at moderate PEEP levels with lower tidal volumes. The spatial resolution of OCT is much higher than the resolution of other tomography techniques used for imaging of whole lung mechanics, such as impedance tomography or computer tomography. The sub-10- $\mu\text{m}$  axial resolution of OCT allows identification of single alveoli and acini. In previous studies, analyses of alveolar dynamics during the ventilatory cycle were usually based on microscope images capturing the projections of subpleural alveoli through a cover glass sucked to the pleura. Compared to microscopy, the depth information of OCT provides a new and unique insight into alveolar mechanics. Other than in microscopy, the expansion of the alveoli in the  $z$  direction and their interconnectivity during the different phases of ventilation can be observed with OCT. The depth information helps to avoid possible misinterpretations of the behavior of subpleural alveoli. It has been controversially discussed if surface alveoli are structurally independent of the pleura or if they are tightly tethered to it. Assuming the latter, sucking the pleura to a

cover glass or the overall expansion of the pleura during inflation might influence the local mechanics of the tethered alveoli, making them special and different from more central alveoli. This could lead to a misinterpretation of 2-D expanding alveoli as being well aerated, while in fact they are only stretched by the pleura during inspiration and are not connected to the airways, because the underlying acini are crumbled and folded and the air is trapped inside the alveoli. Because OCT looks deeper into the next two layers, this misinterpretation is omitted. Any interplay between pleura and tethered subpleural alveoli can be observed in relation to the next deeper alveoli.

Although the depth information of OCT is advantageous over microscopy, the penetration depth is still limited to surface and subsurface alveoli, giving access only to a small portion of the whole lung parenchyma. The findings of subpleural alveolar mechanics in correlation to ventilator settings cannot directly be generalized to the whole lung. One might also speculate if the three visible layers of subsurface alveoli still behave mechanically different from deeper alveoli. These speculations can neither be verified nor rejected with OCT or any other currently available imaging technique. Because the limitation of the penetration depth in OCT is caused by the scattering of the probe light within the lung tissue, and especially at the tissue-air interfaces, it is a principal limitation of the OCT technique in imaging aerated lungs.

In this study, a contact gel was used and the lung was kept within the  $z$ -measuring range by the gel covered window of the scanner head. In principle, this contact is not necessary for the OCT measurement and the lung can move freely, if a correction of the  $z$  distance between scanner head and pleura is implemented. OCT measurement tolerates movements of the  $z$  position within its measuring depth, which is much larger than the (sub)micrometer depth of focus in microscopy. Therefore, any necessary correction of the  $z$  position is less critical and there is no need for contact with a cover glass.

The isolated, ventilated, and perfused lung as used in our study is a well established model to study ventilator effects on the onset or development of lung injury. For OCT measurements, it has two practical advantages. First, the OCT scanner head can be moved freely to any position of the lung, allowing comparisons between different (dependent, nondependent) parts of the same lung. Second, as the perfusate is free of blood cells, scattering in the alveolar walls is substantially lowered. The lack of highly scattering erythrocytes in particular guarantees the highest possible penetration depth.

Despite these advantages, one has to be aware of the general limitations of this model, such as the missing effect of the thorax wall onto the lung mechanics during mechanical ventilation. However, even when performing *in-vivo* OCT studies in a whole animal model, the chest would have to be opened to some extent. The missing constriction at the place of measurement would also lead to different mechanical behavior, especially of the subpleural alveoli under investigation. One could speculate about using endoscopic OCT probes placed between the chest wall and the pleura, but this again would detach the pleura from the chest wall and introduce a different kind of mechanical stress on pleura and subpleural alveoli.

During ventilation with a rate of 12 ventilatory cycles per minute, there is only a limited time to capture images of the

different end-inspiratory and end-expiratory phases of ventilation without introducing motion artifacts. One has to compromise between the number of A scans per frame and the frame rate. Our Fourier domain OCT system was capable of capturing 6-mm (600 A scans) wide cross sections in 123 msec. The wide lateral cross sectional area was chosen to obtain a time-resolved overview in which each cross section contains an ensemble of alveoli. Within this ensemble, each individual alveolus is sliced at an arbitrary position with respect to its full diameter. The movement of the lung perpendicular to the slicing plane during ventilation introduces an error into the measurement of the diameter of one individual alveolus from one image to the next. Because of the movement, a change in diameter cannot only be caused by an actual expansion/deflation of the alveolus, but also by a shift into or out of the cross sectional plane. The ensemble of alveoli, however, still gives a correct averaged impression of the alveolar inflation or deflation status. The wide lateral expansion of the cross sections also allows visualizing local differences between areas with alveolar R/D processes and areas with volume change without total collapse of alveoli.

Although the restriction to cross sectional imaging hinders a quantitative analysis of the volume change of individual alveoli during ventilation, the qualitative statements about the dependency of alveolar mechanics on PEEP and tidal volume settings derived from the images hold true.

Of course, a rapid 3-D scanning would make it possible to quantitatively follow the volume change of individual alveoli throughout ventilation. The scanning speed of the 3-D apparatus used in this study for imaging the fixated lungs would have been too slow for real-time imaging. By improving speed, real-time 3-D OCT imaging of individual alveoli will become possible. Using Fourier domain OCT carries the advantage over time domain OCT that the speed is not limited by mechanically moving parts, but only by the read-out rate of the line detector. In addition, FD-OCT has sensitivity advantages over TD-OCT. However, with the FD-OCT there is still a tradeoff between signal-to-noise ratio and speed. Considering the ongoing development of high output power broadband SLD light sources, higher scanning rates at the same SNR level will be possible with a compact FDOCT system. Another prerequisite for fast 3-D OCT is the use of an OCT scanner head with a fast  $x$ - $y$  beam deflection instead of a combination of galvanometer mounted mirror for the  $x$  direction and a translation stage for the  $y$  direction.

In conclusion, it can be stated that FD-OCT is an image modality that is well suited for observing lung mechanics on an alveolar scale during mechanical ventilation. Because of the intrinsic depth information, FD-OCT outperforms microscopy and carries the potential of providing full 3-D image information of the alveolar mechanics during tidal ventilation. The insight into the 500  $\mu\text{m}$  behind the pleura will help to address questions about alveolar mechanics left open by microscopy. Questions like how alveoli and acini unfold and expand into the 3-D space during inflation under different ventilator settings. The answer to this question will help to clarify the amount of mechanical stress put on the alveolar walls and their relation to ventilator settings in the process of ventilator-induced injury. This might finally contribute to the development of more protective forms of ventilation.

### Acknowledgments

The FDOCT system was developed in collaboration with Peter Koch and Dennis Boller (Medical Laser Centre Lübeck, Germany). We thank Axel Heller, Marcello Gama de Abreu, and Sebastian Stehr for the practical introduction into the isolated lung apparatus. We also thank Sabine Böttcher and Björn Fischer for assistance during lung preparation. Financial support of our group was provided by the NBL3 program of the Bundesministerium für Bildung und Forschung (BMBF).

### References

1. D. Huang, E. A. Swanson, C. P. Lin, J. S. Schuman, W. G. Stinson, W. Chang, M. R. Hee, T. Flotte, K. Gregory, C. A. Puliafito, and J. G. Fujimoto, "Optical coherence tomography," *Science* **254**, 1178–1181 (1991).
2. K. F. Udobi, E. Childs, and K. Touijer, "Acute respiratory distress syndrome," *Am. Fam. Physician* **67**, 315–322 (2003).
3. "International consensus conferences in intensive care medicine. Ventilator-associated lung injury in ARDS. American Thoracic Society, European Society of Intensive Care Medicine, Societe de Reanimation Langue Francaise," *Intensive Care Med.* **25**, 1444–1452 (1999).
4. "Ventilation with lower tidal volumes as compared with traditional tidal volumes for acute lung injury and the acute respiratory distress syndrome. The Acute Respiratory Distress Syndrome Network," *N. Engl. J. Med.* **342**, 1301–1308 (2000).
5. J. A. Frank and M. A. Matthay, "Science review: Mechanisms of ventilator-induced injury," *Crit. Care* **7**, 233–241 (2003).
6. D. Carney, J. DiRocco, and G. Nieman, "Dynamic alveolar mechanics and ventilator-induced lung injury," *Crit. Care Med.* **33**, S122–S128 (2005).
7. R. D. Hubmayr, "Perspective on lung injury and recruitment: A skeptical look at the opening and collapse story," *Am. J. Respir. Crit. Care Med.* **165**, 1647–1653 (2002).
8. B. Jonson, "Elastic pressure-volume curves in acute lung injury and acute respiratory distress syndrome," *Intensive Care Med.* **31**, 205–212 (2005).
9. J. Gil, H. Bachofen, P. Gehr, and E. R. Weibel, "Alveolar volume-surface area relation in air- and saline-filled lungs fixed by vascular perfusion," *J. Appl. Physiol.: Respir., Environ. Exercise Physiol.* **47**, 990–1001 (1979).
10. G. K. Wolf and J. H. Arnold, "Noninvasive assessment of lung volume: respiratory inductance plethysmography and electrical impedance tomography," *Crit. Care Med.* **33**, S163–S169 (2005).
11. L. M. Malbouissou, J. C. Muller, J. M. Constantin, Q. Lu, L. Puybasset, and J. J. Rouby, "Computed tomography assessment of positive end-expiratory pressure-induced alveolar recruitment in patients with acute respiratory distress syndrome," *Am. J. Respir. Crit. Care Med.* **163**, 1444–1450 (2001).
12. B. D. Daly, G. E. Parks, C. H. Edmonds, C. W. Hibbs, and J. C. Norman, "Dynamic alveolar mechanics as studied by videomicroscopy," *Respir. Physiol.* **24**, 217–232 (1975).
13. H. J. Schiller, U. G. McCann, D. E. Carney, L. A. Gatto, J. M. Steinberg, and G. F. Nieman, "Altered alveolar mechanics in the acutely injured lung," *Crit. Care Med.* **29**, 1049–1055 (2001).
14. G. Häusler and M. W. Lindner, "Coherence radar and spectral radar—New tools for dermatological diagnosis," *J. Biomed. Opt.* **3**(1), 21–31 (1998).
15. A. F. Fercher, C. K. Hitzenberger, G. Kamp, and S. Y. El-Zaiat, "Measurement of intraocular distances by backscattering spectral interferometry," *Opt. Commun.* **117**, 43–48 (1995).
16. A. F. Fercher, W. Drexler, C. K. Hitzenberger, and T. Lasser, "Optical coherence tomography—Principles and applications," *Rep. Prog. Phys.* **66**, 239–303 (2003).
17. B. Cense, N. A. Nassif, T. C. Chen, M. C. Pierce, S. H. Yun, B. H. Park, B. E. Bouma, G. J. Tearney, and J. F. de Boer, "Ultra-high-resolution high-speed retinal imaging using spectral-domain optical coherence tomography," *Opt. Express* **12**, 2435–2447 (2004).
18. P. Hsiung, Y. Chen, T. H. Ko, J. G. Fujimoto, C. J. S. de Matos, S. V. Popov, J. R. Taylor, and V. P. Gapontsev, "Optical coherence tomography using a continuous-wave, high-power, Raman continuum light

- source," *Opt. Express* **12**, 5287–5295 (2004).
19. K. W. Gossage, T. S. Tkaczyk, J. J. Rodriguez, and J. K. Barton, "Texture analysis of optical coherence tomography images: Feasibility for tissue classification," *J. Biomed. Opt.* **8**(3), 570–575 (2003).
  20. Y. Yang, S. Whiteman, D. G. van Pittius, Y. He, R. K. Wang, and M. A. Spiteri, "Use of optical coherence tomography in delineating airways microstructure: Comparison of OCT images to histopathological sections," *Phys. Med. Biol.* **49**, 1247–1255 (2004).
  21. S. A. Boppart, J. Herrmann, C. Pitris, D. L. Stamper, M. E. Brezinski, and J. G. Fujimoto, "High-resolution optical coherence tomography-guided laser ablation of surgical tissue," *J. Surg. Res.* **82**, 275–284 (1999).
  22. N. Hanna, D. Saltzman, D. Mukai, Z. Chen, S. Sasse, J. Milliken, S. Guo, W. Jung, H. Colt, and M. Brenner, "Two-dimensional and 3-dimensional optical coherence tomographic imaging of the airway, lung, and pleura," *J. Thorac. Cardiovasc. Surg.* **129**, 615–622 (2005).
  23. M. G. de Abreu, M. Heintz, A. Heller, R. Szechenyi, D. M. Albrecht, and T. Koch, "One-lung ventilation with high tidal volumes and zero positive end-expiratory pressure is injurious in the isolated rabbit lung model," *Anesth. Analg. (Baltimore)* **96**, 220–228 (2003).
  24. T. Koch, H. P. Duncker, S. Rosenkranz, H. Neuhof, and A. K. Van, "Alterations of filtration coefficients in pulmonary edema of different pathogenesis," *J. Appl. Physiol.* **73**, 2396–2402 (1992).